Heliyon 7 (2021) e06958

Contents lists available at ScienceDirect

Heliyon

journal homepage: www.cell.com/heliyon

Research article

Spectroscopic and structural properties of CeO_2 nanocrystals doped with La^{3+}, Nd^{3+} and modified on their surface with Ag nanoparticles

Monika Michalska [a,b,*], Karol Lemański [c], Andrzej Sikora [d]

[a] Łukasiewicz Research Network - Institute of Microelectronics and Photonics, Al. Lotników 32/46, 02-668 Warsaw, Poland
[b] Department of Chemistry, Faculty of Materials Science and Technology, VŠB-Technical University of Ostrava, 17. Listopadu 15/2172, 708 00 Ostrava-Poruba, Czech Republic
[c] Institute of Low Temperature and Structure Research, Polish Academy of Sciences, Okólna 2, 50-422 Wrocław, Poland
[d] Faculty of Microsystem Electronics and Photonics, Wroclaw University of Science and Technology, Janiszewskiego 11/17, 50-372 Wrocław, Poland

ARTICLE INFO

Keywords:
Cerium dioxide
CeO_2
Silver nanoparticles
Lanthanides
Spectroscopy

ABSTRACT

The purpose of this work is to present our efforts focused on applications of chemical synthesis of nanocrystalline cerium dioxide (CeO_2) powders doped with La^{3+} ions and CeO_2:Nd^{3+} modified, on their surface, with Ag nanoparticles (NPs). The synthesized powders were examined by X-ray powder diffraction (XRD), absorption, emission spectroscopy, scanning electron (SEM) and atomic force microscopy (AFM). The relations between crystallographic properties and stability of CeO_2 compounds doped by La ions and surface-modified by Ag were studied. XRD patterns revealed that all studied samples are single-phase and crystallized in the cubic fluorite-type structure, in space group Fm-3m. The average crystallite sizes estimated by Rietveld method of series: La-doped CeO_2 were in the range of 7–14 nm, and CeO_2:1%Nd^{3+}/n-Ag (n: 1- 5wt.%) were found to be in the range of 29–34 nm, respectively. The lattice parameter *a* for La-doped CeO_2 powders varying from 5.416 to 5.482 Å with increasing content of La^{3+} ions from 0 to 20wt.%, respectively. For series of CeO_2:Nd^{3+}/n-Ag materials lattice parameter *a* was at the same level and in accordance with the standard value $a_0 = 5.411$ Å (ICDD - 43-1002). The SEM and AFM observations depicted the grainy structure of all obtained CeO_2-powder samples. The estimated grain size ranged from 50 to 500 nm. The diverse grain shapes and packing was remarked in the samples. According to our knowledge, the relationship between the structural, spectroscopic and morphological characteristics of CeO_2 samples was presented in this work for the first time.

1. Introduction

The most stable modification of cerium dioxide, CeO_2, crystallizes in the fluorite-type structure, space group Fm-3m [1]. The CeO_2 compounds, due to its unique properties, have been widely used in various applications, e.g.: supercapacitors [2, 3, 4], solid oxide fuel cells (SOFC) [5, 6, 7], solar cells [8, 9, 10], catalytic [11, 12, 13, 14], gas sensing [15, 16] and corrosion protection [17, 18].

By changing the grain size, especially for nanosized compounds, new properties can be obtained and, as a result, new applications can be found [19, 20]. As to CeO_2 nanoparticles, it was shown that a decrease in the size stays in relation to a significant increase in the cell parameter [21, 22, 23]. The ferromagnetism as well as the other magnetic properties of CeO_2 depends also on its particles size [24, 25]. It was shown in the literature, that La^{3+} considerably improves the catalytic activity of CeO_2 for soot oxidation by O_2 [26]. For La-doped NPs, it was found, that both the dopant (La^{3+}) and Ce^{3+} were distributed homogeneously throughout the particles [27]. CeO_2 nanostructures are interesting materials, also due to their ability for strong UV radiation absorption and the potential excitation of the doped optically active ions by energy transfer. Surface modification of CeO_2 with Ag nanoparticles have positive effect in the photocatalysis experiments realized under visible light irradiation of the degradation of 4-nitrophenol and methylene blue than pristine CeO_2 material [28, 29].

A variety of approaches were developed to achieve at the same time a single-phase, ultrafine and homogenous CeO_2 materials in the form of powder or thin films, such as: solid-state synthesis [30], sol-gel [31, 32], precipitation [31, 32, 33, 34, 35, 36, 37], combustion [38, 39, 40], hydrothermal [41, 42, 43], solvothermal [44, 45], microemulsion [46, 47], electrochemical deposition [48] and so on.

* Corresponding author.
E-mail address: michalska.monika83@gmail.com (M. Michalska).

https://doi.org/10.1016/j.heliyon.2021.e06958
Received 22 November 2020; Received in revised form 13 March 2021; Accepted 26 April 2021

In this contribution, we present the structural, morphological and spectroscopic studies on CeO_2 nanocrystals doped with La^{3+} or Nd^{3+} ions, and modified CeO_2:Nd^{3+} on their surface with Ag metals. The correlation between the structural, morphological and spectroscopic properties of CeO_2 nanocrystals doped with Nd^{3+} ions and modified on their surface with silver metallic nanoparticles was examined for the first time. To the best of our knowledge, this is also the first case of the utilization of atomic force microscopy (AFM) to observe the difference between the nanocrystalline powders of CeO_2 with and without modified surface. In this work, the nanocrystalline CeO_2 powders doped with La^{3+} ions were prepared using a modified sol-gel process, and the surface-modified commercial CeO_2 particles with 1–5%wt.Ag were fabricated using the low-temperature chemical synthesis. The structural features were examined by X-ray powder diffraction, absorption, emission spectroscopy, scanning electron and atomic force microscopy. As the result, the structural, morphological and spectroscopy studies performed in this work were carried out to assess the readiness in terms of the verification of the usefulness of CeO_2 nanocrystalline powders as a potential material for application in UV light detection, which transfer energy (in the UV region) to the doped rare earth ions.

2. Experimental

2.1. Synthesis of CeO_2 doped with La^{3+} ions

High pure cerium (III) nitrate hexahydrate ($Ce(NO_3)_3 \cdot 6H_2O$ from Sigma-Aldrich, 99.99%), lanthanum (III) nitrate hexahydrate ($La(NO_3)_3 \cdot 6H_2O$ from Sigma-Aldrich, 99.99%), citric acid monohydrate ($C_6H_8O_7 \cdot H_2O$, pure p.a., 99.5% from Avantor Performance Materials Poland S.A), acetic acid ($C_2H_4O_2$ from CHEMPUR, 99.5%) were utilized to obtain CeO_2 nanocrystalline powders doped with 5, 10 and 20% wt. of La ions. The nominal Ce:La molar composition ratios were 1.95:0.05, 0.9:0.1 and 0.8:0.2.

Stoichiometric amounts of cerium and lanthanum nitrates were separately turned from solid to liquid phases in deionized water under continuous magnetic stirring. Then, the cerium and lanthanum water salt solutions were mixed together and, followingly citric and acetic acids were slowly dropped into the solutions. The excess water was evaporated very slowly from the properly prepared solutions until gels were formed. The gel precursors created in the preceding process were air-dried at 150 °C for a few hours. The pre-dried powders so-called xerogels were calcined in a one-stage process between 300 °C and 500 °C for the few hours in an air atmosphere.

2.2. Synthesis of CeO_2 modified with Ag NPs and Nd^{3+} ions

To synthesize the CeO_2/n-Ag composites, silver nitrate ($AgNO_3$, pure, Avantor Performance Materials Poland S.A) was first dissolved in ethanol (96%, Avantor Performance Materials Poland S.A) solution. Then, the cerium (IV) oxide (CeO_2, ≥99.0%, ca. 1% of impurities of Nd^{3+} ions, Aldrich) powder was introduced into to the silver nitrate solution to obtain a suspension ($AgNO_3$–EtOH–H_2O–CeO_2) under continuous magnetic stirring process. Appropriate weight ratio: 0.01, 0.02, 0.03, 0.04 and 0.05 of Ag and CeO_2 was used. To obtain a homogeneously dispersed suspension, the resulting mixture was magnetically stirred for several hours. Lately, to remove excess alcohol and water from the suspension the conditions of air-dried at 150 °C for a few hours was utilized. In order to obtain a fine powders, the so-obtained composites in an agate mortar were grounded [49, 50, 51, 52, 53].

2.3. Measurements

XRD analysis was utilized as a pivotal technique to recognize the crystalline phase of the prepared powders. The XRD patterns were acquired in angle range from 10° to 60° (2θ angle) using a Siemens D-500 X-ray powder diffractometer equipped with a Cu K_α radiation source, emitting λ = 1.542 Å. The phase analysis as well as the structural parameters refinement performed using Rietveld method were acquired using a PDF4+2019 database.

The absorption spectra were recorded using a Cary 5000 spectrophotometer. The emission spectra were acquired using a Hamamatsu spectrometer. As an excitation source, the fourth harmonic (266 nm) of Q-switched Nd:YAG pulsed laser was used.

The morphology as well as the particle size of the products were observed and measured using scanning electron microscopy (SEM, Cross Beam Auriga, Carl Zeiss).

The atomic force microscopy measurements were performed using a Dimension 3000 system from Digital Instruments Company. The Tapping Mode was enabled, and the scanning process was carried out at ambient conditions (temperature: 25 °C, relative humidity: 35%). The device was equipped with a 100 μm × 100 μm scanner, which was calibrated using a typical silicon grid provided by NT-MDT. The probes used in the measurements were provided by Nanosensor company. Pointprobes type was utilized, having the parameters as follows: nominal tip radius r_{tip} = 10 nm, resonance frequency range f_{res} = 306–353 kHz, and spring constant k = 43–68 N m^{-1}. The data processing was performed using the SPIP software providing by Image Metrology company [54]. Next to standard 2D surface images, the Sobel transform was provided, as it reveals subtle morphological details. This image processing tool was successfully used in many previous works [55, 56, 57, 58, 59, 60].

3. Results and discussion

3.1. XRD measurements results

The crystal cubic fluorite-type of space group Fm-3m structure of the CeO_2 compound is presented in Figure 1. One can notice, that each cerium (IV) ion (Ce^{4+}) is coordinated by eight oxygen (O^{2-}) ions.

The collected XRD patterns of the pristine and La-doped CeO_2 powders are presented in Figure 2 (A, B). The XRD analysis indicates that all synthesized La-doped CeO_2 powders (Figure 2) are single-phase and they crystallized in the cubic fluorite-type structure, space group Fm-3m, and no other phases are observed in the diffraction patterns. All diffraction peaks are indexed to the cubic structure of cerium (IV) oxide (ICDD - 43-1002) [61,62]. The XRD patterns of the La-doped CeO_2 powders present 5 characteristic peaks for CuK_α radiation (λ = 1.542 Å), which correspond to the crystal planes of (111), (200), (220), (311) and (222), as given in Figure 2. The average crystallite sizes of La-doped CeO_2 estimated by Rietveld method were in the range of 7–14 nm. The cell parameter in La-doped CeO_2 powders increases with the doping concentration of La ions. This relation is correlated with the ionic size of the La-ions (dopant). It also means that the doping of La-ions affects the crystal structure of pristine CeO_2 (see Table 1). To understand the doping on La ions into CeO_2 host structure we decided to closer look at the

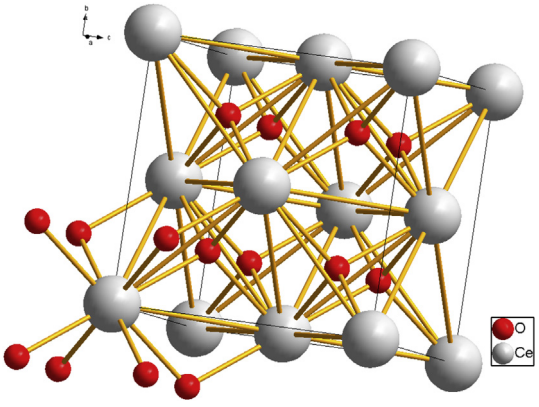

Figure 1. Visualization of the crystal CeO_2 structure with the cubic space group of Fm-3m (225), (ICDD – 43-1002).

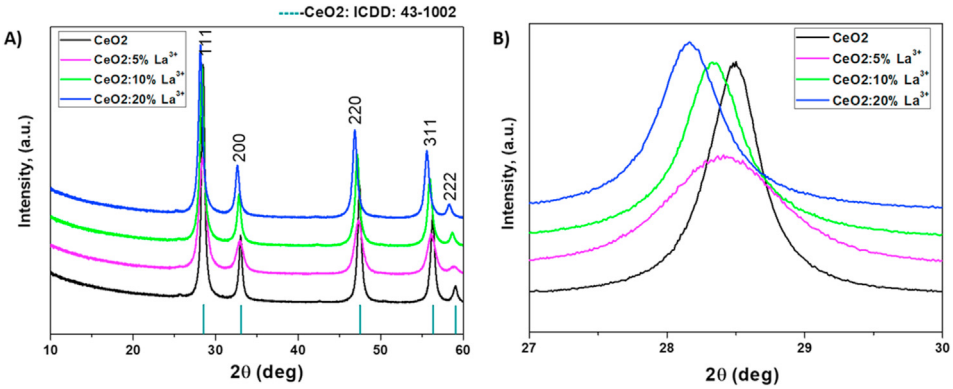

Figure 2. Full-angle (2θ: 10–60°) XRD experimental diffraction patterns of pristine CeO_2 and La-doped samples (2θ: 10–60°) with reference lines of matching CeO_2 phase from a database (A), and narrow angular range (2θ: 27–30°) for (111) diffraction lines (B).

Table 1. Crystallite sizes and cell parameters of pristine and n-La doped CeO_2, as acquired from XRD measurements.

Material	Average crystallite size (XRD), nm	Lattice parameter *a*, Å	Cell volume, Å^3
A) pristine	14	5.4163 (2)	158.90 (1)
B) doped 5% wt. La	7	5.4324 (2)	160.32 (1)
C) doped 10% wt. La	10	5.4506 (2)	161.93 (1)
D) doped 20% wt. La	10	5.4823 (2)	164.78 (1)

changes that could take place in the narrow angular range from 27 to 30° (2θ) at the (111) crystal planes. The slight shift towards lower values of 2θ from 28.5 to 28.2° (2θ) for pristine CeO_2, and CeO_2:10%La^{3+} was observed (Figure 2B). This appearance has been confirmed in other works [63, 64, 65, 66, 67]. It could be assumed according to other researchers and studies, that this phenomenon is connected to estimated i) very small crystallite sizes of synthesized materials by modified sol-gel method what is connected to use to the synthesis conditions, like i.e.: temperature, time, atmosphere, complexing agents, pH, etc., ii) created during synthesis oxygen vacancies and the stacking defects in ceria as well as, iii) structural defects, which originating the stress within the crystal lattice and influencing on the minor shift observed on the XRD peaks at (111) diffraction lines towards lower angles [63, 64, 65, 66, 67].

The XRD patterns of pure and silver-decorated CeO_2:1%wt. Nd^{3+} powders are presented in Figure 3 (A, B). For each sample (see Figure 3A), all peaks are attributed to cerium (IV) oxide structure (ICDD - 43-1002), confirming that the decoration surface of pristine CeO_2 does not lead to any phase segregation. No significant change during performing structural analysis in the Ag content was noticed. The average crystallite sizes of CeO_2 achieved by the Rietveld method, were in the range from 29 to 34 nm. In the result, due to the very low peak intensity caused by the low silver weight content, it was not possible to estimate from the XRD data the crystallite size of Ag nanoparticles. Similar to previous set of ceria-samples, narrow angular range from 27 to 30° (2θ) at the (111) crystal planes was studied (Figure 3B). The shift effect to lower angles was very small and ranged from 28.6 to 28.5° (2θ) for commercial CeO_2, and surface modified with 5%Ag, respectively (Figure 3B). This observation showing and comparing the results of pristine CeO_2 prepared by modified sol-gel method, and commercial CeO_2 material. The estimated lattice parameters and cell volumes for both mentioned samples is almost the same. It is clearly shown, that formation of nanostructures causes the creation of oxygen vacancies, defects and other structural strains [63, 64, 65, 66, 67].

The unit cell parameters and the volumes of all obtained CeO_2 doped with La-ions and modified with Ag NPs calculated from the XRD data are coherent with the typical values (a_0 = 5.411 Å, V_0 = 158.46 Å^3) of the ICDD PDF card. The calculated crystallite sizes, cell parameters and cell volumes for all powders are presented in Table 1 and Table 2. It should be also pointed here that the nanocrystalline CeO_2 material synthesized by modified sol-gel method has smaller average crystallite size and does not have any impurities in comparison with commercial CeO_2 contaminated with Nd^{3+} ions.

3.2. Absorption and emission spectra

The absorption spectra of pure CeO_2 and La^{3+}-doped CeO_2 nanocrystals are similar to each other (Figure 4).

The broad absorption bands are observed from the ultraviolet (UV) up to the blue region, at about 450 nm. From around 500 nm to the near-infrared (NiR) range, the absorption does not occur, so the spectra are

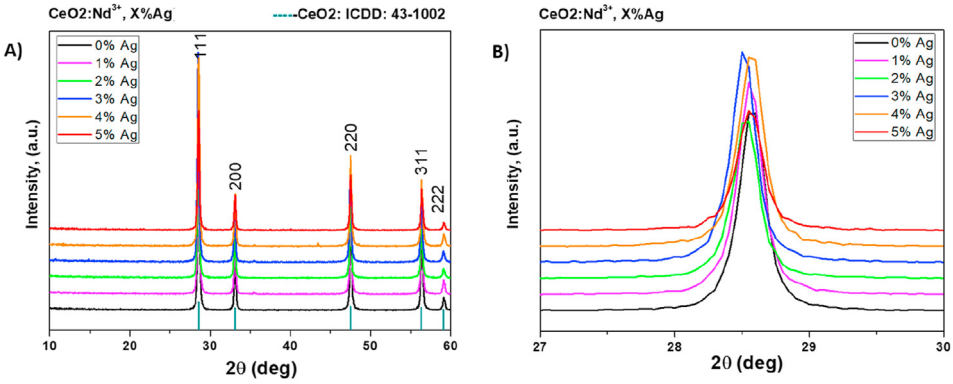

Figure 3. Full-angle range (2θ: 10–60°) XRD experimental diffraction patterns of commercial CeO_2:1%wt. Nd^{3+} with X%Ag with reference lines of matching CeO_2 phase from database (A), and narrow angular range (2θ: 27–30°) for (111) diffraction lines (B).

Table 2. Crystallite sizes and cell parameters of commercial and n-Ag modified CeO_2, as enumerated from XRD measurements.

Material	Average crystallite size (XRD), nm	Lattice parameter *a*, Å	Cell volume, Å^3
A) pristine	29	5.414 (1)	158.71 (5)
B) 1% n-Ag	34	5.412 (1)	158.54 (6)
C) 2% n-Ag	31	5.411 (1)	158.44 (4)
D) 3% n-Ag	31	5,411 (1)	158.46 (6)
E) 4% n-Ag	31	5.412 (1)	158.51 (4)
F) 5% n-Ag	30	5.412 (1)	158.49 (7)

flat. The CeO_2 UV absorption bands are characteristic for this material. The similar absorption spectra were earlier reported for CeO_2 [28-29, 68-70]. Strong ultraviolet absorption capability of cerium oxide is related to the charge transfer from O^{2-} to Ce^{4+} ions. For commercial CeO_2 powders surface modified with Ag NPs and containing 1% of Nd^{3+} ions, the absorption spectra possess similar, but more clearly separated bands in the UV range (with the separation at about 310 nm). The absorption of Ag metallic nanoparticles is observed in the broad region over 450–600 nm. This band does not occur for the commercial CeO_2 powder and is more raised for the samples with a higher amount of Ag NPs (from 3% Ag, see Figure 5).

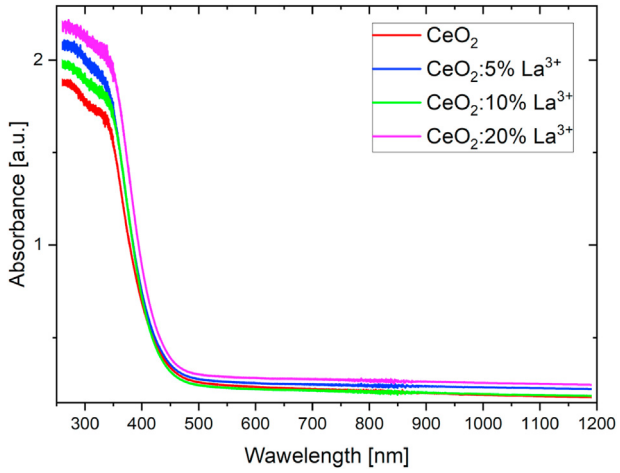

Figure 4. The absorption spectra of pure CeO_2 and La^{3+}-doped CeO_2 nanocrystals.

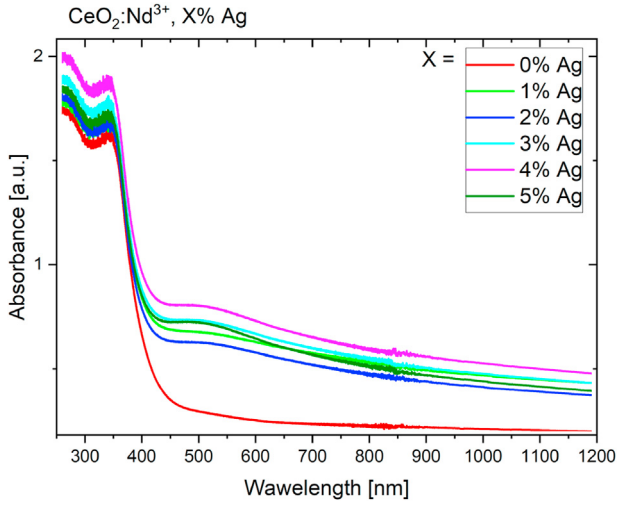

Figure 5. The absorption spectra of CeO_2:1% Nd^{3+}, Ag nanocrystals.

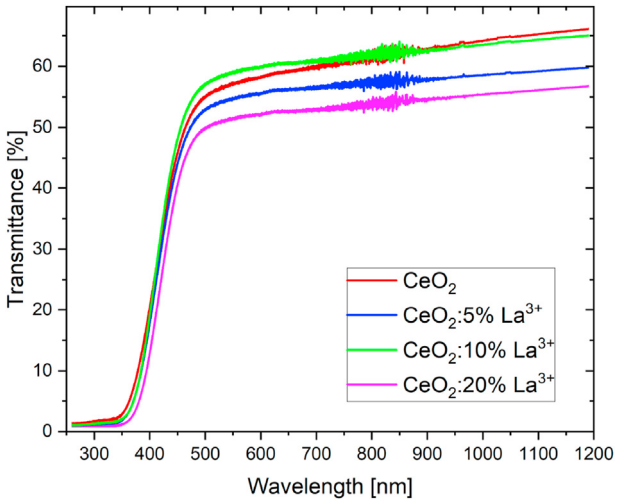

Figure 6. The transmittance spectra of CeO_2 nanocrystals doped with the La^{3+} ions.

The Ag absorption is very sensitive to the local structure environment and related absorption band may appear in different spectral regions, from UV to NiR range [71]. Further luminescence analysis shows that the commercial CeO_2 (with 1% of impurities) is contaminated by some amount of Nd^{3+} ions. The content of Nd^{3+} was too small to be observed in the absorption spectra and XRD patterns.

The transmittance spectra (Figures 6 and 7) were obtained by the mathematical conversion of the measured absorbance, by using the equation:$A = -\log_{10} T$, where A is the absorbance and T is the transmittance. As seen in Figure 6, for the CeO_2 doped with La^{3+} ions, there are no significant differences for different doping levels. The transmission in the visible region is about 50–60 %. For the CeO_2 nanocrystals surface modified with silver NPs, the optical transmission is significantly lower than that in the commercial CeO_2 sample and reaches up to about 30 %. In this compound, Ag nanoparticles possess a higher ability to absorb light than La^{3+} ions.

The energy band gap for each CeO_2 sample was determined by using the Kubelka-Munk method [72], basing on Eq. (1):

$$F(R) = \frac{(1-R)^2}{2R} \quad (1)$$

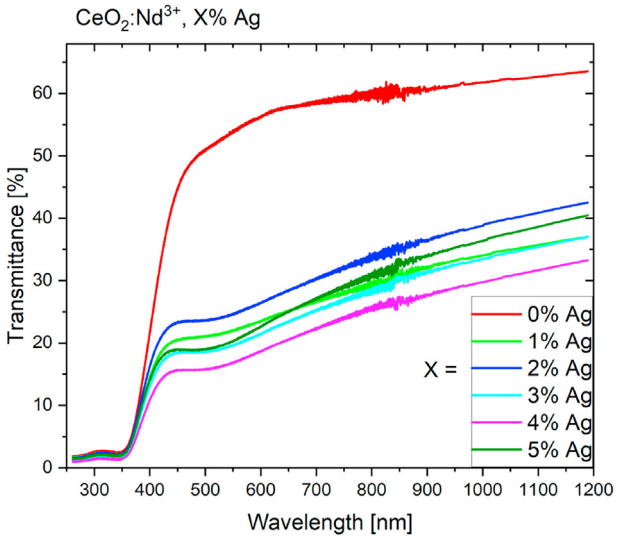

Figure 7. The transmittance spectra of CeO_2:1% Nd^{3+}, Ag nanocrystals.

where R is the reflectance and F(R) is proportional to the extinction coefficient. After multiplying the F(R) function by *hν* and using coefficient *n*, associated with electronic transition type (in this case n = 2, for an indirect allowed transition), Eq. (2) is obtain:

$$(\boldsymbol{F}(\boldsymbol{R})*\boldsymbol{h\nu})^{\boldsymbol{n}} \quad (2)$$

By plotting this equation as a function of the energy in eV, the band gap energy (E_g) can be received (see Figure 8).

The calculations were done for ten samples of CeO_2 (with or without dopants, or surface modification) and, as an example, the plotting for the CeO_2 surface modified with Ag NPs is given in Figure 8. The results were the same for all investigated samples; the energy band gaps were equal to about 3.4 eV (Figure 8). The obtained result is within the range of band gap values reported for CeO_2 in the literature (3.0–3.6 eV) [73].

The emission spectra are characteristic of the Nd^{3+} ions. The excitation was at 266 nm, so the host lattice of CeO_2 transfers energy to the Nd^{3+} ions. The most intensive emission peak is observed at 901 nm, which corresponds to the energy of 11099 cm^{-1} and represents the $^4F_{3/2} \rightarrow {}^4I_{9/2}$ transition [74, 75, 76]. The emission from the transition $^4F_{3/2} \rightarrow {}^4F_{11/2}$ is also observed, as well as the weak emission from the $^4F_{5/2}+{}^2H_{11/2}$ multiplets (see Figure 9).

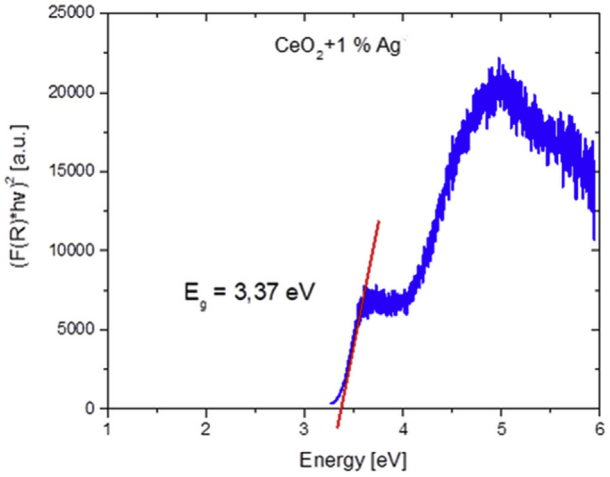

Figure 8. Graphical visualization of the Kubelka-Munk formula with estimation of the energy bandgap for the investigated cerium (IV) oxide.

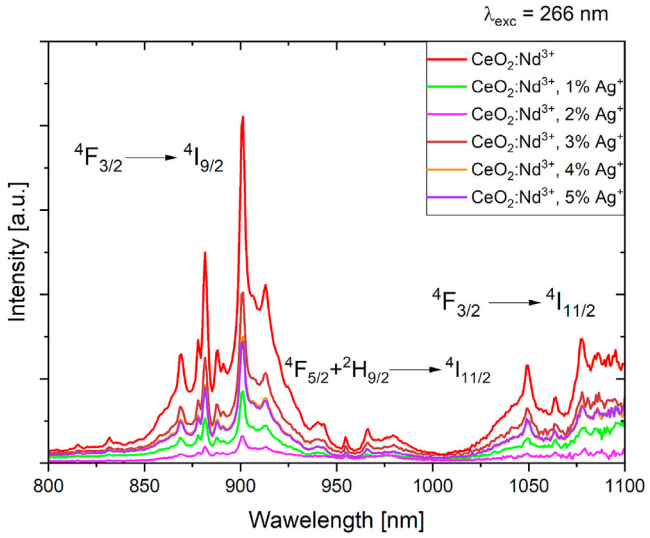

Figure 9. Near Infrared emission spectra of the CeO_2: Nd^{3+}, Ag nanocrystals.

The most intensive emission possesses the sample without Ag. This phenomenon may be due to the luminescence quenching mechanisms, which occur in this case when Nd^{3+} ions non-radiatively transfer their energy to the silver nanoparticles.

3.3. Morphological properties

The SEM pictures of all obtained powders are depicted in Figure 10. All powders show agglomerates, consisting of smaller grains (10–50 nm) - series of CeO_2 doped with La^{3+} ions, and of 50 nm to few micrometer-sized grains – series of CeO_2 with Ag NPs and Nd^{3+} ions.

The AFM results are presented as a set of images in Figure 11. It should be emphasized that the number of AFM measurements was performed for each sample to provide representative results. The grainy structure is clearly noticeable for all samples. The typical grain size varies in the range of 50–500 nm. Despite the fact that normally grainy materials tend to agglomerate, some specific grains ordering can be observed. In the 2A – CeO_2+5%La^{3+} sample, they are created as a high-density pack, locally showing complete fill, as the almost flat surface is created. In the 2B – CeO_2+1%Ag sample, the high aspect ratio structures (some microns in length and hundreds of nanometers in diameter) can be seen. For many samples, the amount of grains becomes bigger while their size decreases (tens of nanometers). In the sample 4B – CeO_2+3%Ag, a large particle with flat surface covered with agglomerates of particles and single particles was found. It appears that they cover large grains of micrometer diameter, or create such large agglomerates. Except for 2B – CeO_2+1%Ag and 4B – CeO_2+3%Ag samples, no specific structure orientation was noticed. It is noted that the steep structures were not imaged properly, and, as it is typical for AFM scans, the side of the scanning tip influence was revealed (sample 3A – CeO_2+10%La^{3+}). One can also notice that, while the metal content increases, the materials become more bulky, with smaller spaces and voids. The shape of grains is much better fit to each other in 3D space also in terms of shape. This feature is more visible in the case of silver than lanthanum addition. Simultaneously, the filling factor increase is related to the grain shapes. More square-like features instead of round ones makes the space filling more effective and easy. Those particular properties may have an impact on both mechanical and electrical properties, while it eliminates the content of weak bonds between the particles as well as poor electrical conductivity and capacitance-based charge transport. The developed metallic grains covering with optimal shapes determines also the optical properties, causing increased radiation absorption.

4. Conclusions

In this work, the nanocrystalline CeO_2 powders doped with La^{3+} ions were prepared using the modified sol-gel process. Also, the commercial CeO_2 particles surface-modified with 1–5% wt. Ag NPs and co-doped with Nd^{3+} ions were synthesized using the low-temperature chemical synthesis. The synthesized samples were phase-pure and they have the cubic CeO_2-type crystal structure in space group Fm-3m. The average crystallite size estimated by the Rietveld method were in the range of 7–14 nm (La-doped CeO_2) and 29–34 nm (CeO_2:1%Nd^{3+}/n-Ag (n: 1- 5wt.%)) for the modified sol-gel and low-temperature chemical syntheses, respectively. The SEM and AFM studies revealed the grainy structure of all obtained powder samples. The grain size varied in the range of 50–500 nm. The diverse grain shapes and packing was observed in the samples. The main light absorption of pure and doped CeO_2 lies in the near-ultraviolet area, due to the strong charge transfer from O^{2-} to Ce^{4+} ions. The investigated samples may find future applications, e.g., for UV light detection and as materials with efficient transfer energy (in the UV region) to the doped rare earth ions.

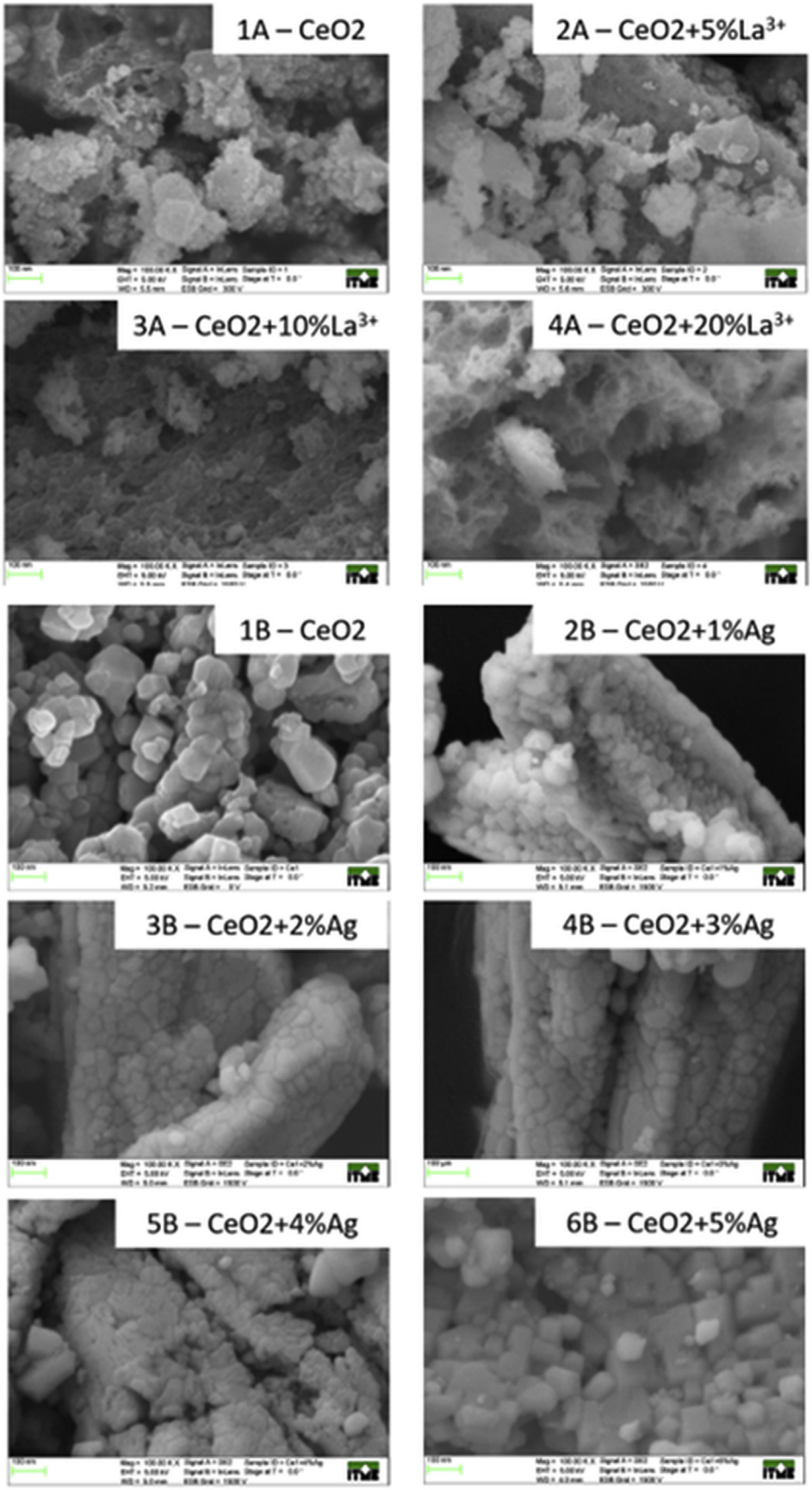

Figure 10. The SEM images of all obtained CeO_2 powders.

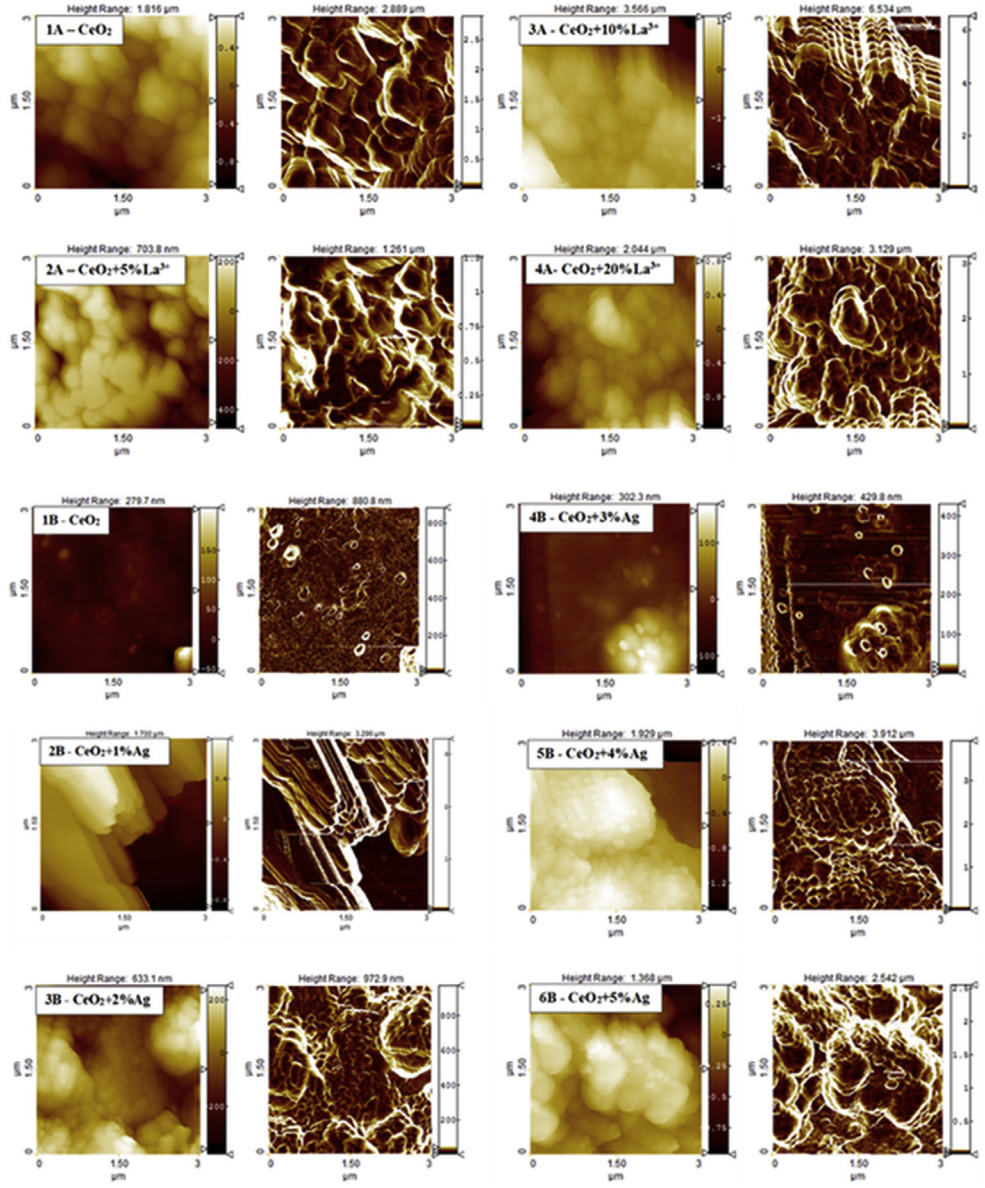

Figure 11. AFM images of all investigated samples. Left hand side – topography, right hand side – Sobel transform.

Declarations

Author contribution statement

Monika Michalska: Conceived and designed the experiments; Performed the experiments; Analyzed and interpreted the data; Contributed reagents, materials, analysis tools or data; Wrote the paper.

Karol Lemański, Andrzej Sikora: Performed the experiments; Analyzed and interpreted the data; Contributed reagents, materials, analysis tools or data; Wrote the paper.

Funding statement

This work was financially supported by the National Centre for Research and Development through the research project cooperation between the National Centre for Research and Development (NCBR) and the Ministry of Science and Technology of Taiwan (MOST) (contract no. PL-TW/IV/6/2017).

Data availability statement

Data will be made available on request.

Declaration of interests statement

The authors declare no conflict of interest.

Additional information

No additional information is available for this paper.

References

[1] M. Malathi, K. Sreenu, G. Ravi, P.V. Kumar, C.S. Reddy, R. Guje, R. Velchuri, M. Vithal, Low temperature synthesis of fluorite-type Ce-based oxides of

composition $Ln_2Ce_2O_7$ (Ln = Pr, Nd and Eu): photodegradation and Luminescence studies, J. Chem. Sci. 129 (2017) 1193–1203.
[2] Y. Luo, T. Yang, Q. Zhao, M. Zhang, CeO_2/CNTs hybrid with high performance as electrode materials for supercapacitor, J. Alloys Compd. 729 (2017) 64–70.
[3] L.S. Aravinda, K. Udaya Bhat, Badekai Ramachandra Bhata, Nano CeO_2/activated carbon based composite electrodes for high performance supercapacitor, Mater. Lett. 112 (2013) 158–161.
[4] H. Heydari, M.B. Gholivand, A novel high-performance supercapacitor based on high-quality CeO_2/nitrogen-doped reduced graphene oxide nanocomposite, Appl. Phys. A 123 (2017) 187.
[5] J.-H. Wang, M.L. Liu, M.C. Lin, Oxygen reduction reactions in the SOFC cathode of Ag/CeO_2, Solid State Ionics 177 (2006) 939–947.
[6] M.K. Chinnu, K.V. Anand, R.M. Kumar, T.A. Alagesan, R. Jayavel, Formation and characterisation of CeO_2 and Gd:CeO_2 nanowires/rods for fuel cell applications, J. Exp. Sci. 10 (2015) 520–531.
[7] D. Kashyap, P.K. Patro, R.K. Lenka, T. Mahata, P.K. Sinha, Effects of Gd and Sr co-doping in CeO_2 for electrolyte application in solid oxide fuel cell (SOFC), Ceram. Int. 40 (2014) 11869–11875.
[8] C.E. Milliken, S. Guruswamy, A.C. Khandkar, Electrochemical stability of strontium-doped ceria electrolyte in solid-oxide fuel cell applications, J. Am. Ceram. Soc. 84 (2001) 1533–1538.
[9] S.V. Umale, S.N. Tambat, S.M. Sontakke, Combustion synthesized CeO_2 as an anodic material in dye sensitized solar cells, Mater. Res. Bull. 94 (2017) 483–488.
[10] J. Roh, S.H. Hwang, J. Jang, Dual-Functional CeO_2:Eu^{3+} nanocrystals for performance-enhanced dye-sensitized solar cells, Appl. Mater. Interf. 6 (2014) 19825–19832.
[11] T. Montini, M. Melchionna, M. Monai, P. Fornasiero, Fundamentals and catalytic applications of CeO_2-based materials, Chem. Rev. 116 (2016) 5987–6041.
[12] A. Rangaswamy, P. Sudarsanam, B.M. Reddy, Rare earth metal doped CeO_2-based catalytic materials for diesel soot oxidation at lower temperatures, J. Rare Earths 33 (2015) 1162–1169.
[13] B.M. Reddy, L. Katta, G. Thrimurthulu, Novel nanocrystalline $Ce_{1-x}La_xO_{2-\delta}$ (x = 0.2) solid solutions: structural characteristics and catalytic performance, Chem. Mater. 22 (2010) 467–475.
[14] H. Li, G. Lu, Y. Wang, Y. Guo, Y. Guo, Synthesis of flower-like La or Pr-doped mesoporous ceria microspheres and their catalytic activities for methane combustion, Catal. Commun. 11 (2010) 946–950.
[15] H.-J. Beie, A. Gnörich, Oxygen gas sensors based on CeO_2 thick and thin films, Sensor. Actuator. B Chem. 4 (1991) 393–399.
[16] L. Liao, H.X. Mai, Q. Yuan, H.B. Lu, J.C. Li, C. Liu, C.H. Yan, Z.X. Shen, T. Yu, Single CeO_2 nanowire gas sensor supported with Pt nanocrystals: gas sensitivity, surface bond states, and chemical mechanism, J. Phys. Chem. C 112 (2008) 9061–9065.
[17] D. Ghosh, S. Mukherje, S. Das, Ceria (CeO_2) based coating for high temperature corrosion protection of 9Cr-1 Mo steel, Protect. Met. Phys. Chem. Surface 51 (2015) 441–447.
[18] T. Chen, D. Liu, F. Wu, H. Wang, Effect of CeO_2 on microstructure and wear resistance of TiC bioinert coatings on Ti_6Al_4V alloy by laser cladding, Materials 11 (2018) 58.
[19] P.J. Dereń, K. Lemański, A. Gągor, A. Watras, M. Małecka, M. Zawadzki, Symmetry of $LaAlO_3$ nanocrystals as a function of crystallite size, J. Solid State Chem. 183 (2010) 2095.
[20] P.J. Dereń, K. Lemański, On tuning the spectroscopic properties of $LaAlO_3$:Pr^{3+} nanocrystallites, J. Lumin. 131 (2011) 445.
[21] J.E. Spanier, R.D. Robinson, F. Zhang, S.-W. Chan, I.P. Herman, Size-dependent properties of CeO_{2-y} nanoparticles as studied by Raman scattering, Phys. Rev. B 64 (2001) 245407.
[22] S. Tsunekawa, R. Sahara, Y. Kawazoe, K. Ishikawa, Lattice relaxation of monosize CeO_{2-x} nanocrystalline particles, Appl. Surf. Sci. 152 (1999) 53.
[23] S. Tsunekawa, K. Ishikawa, Z.-Q. Li, Y. Kawazoe, Y. Kasuya, Origin of anomalous lattice expansion in oxide nanoparticles, Phys. Rev. Lett. 85 (2000) 3440.
[24] Y. Liu, Z. Lockman, A. Aziz, J. MacManus-Driscoll, Size dependent ferromagnetism in cerium oxide (CeO_2) nanostructures independent of oxygen vacancies, J. Phys. Condens. Matter 20 (2008) 165201.
[25] K. Ackland, J.M.D. Coey, Room temperature magnetism in CeO_2—a review, Phys. Rep. 746 (2018) 1–39.
[26] A. Bueno-López, K. Krishna, M. Makkee, A. Moulijn, Enhanced soot oxidation by lattice oxygen via La^{3+}-doped CeO_2, J. Catal. 230 (2005) 237–248.
[27] W. Lee, S.-Y. Chen, E. Tseng, A. Gloter, C.-L. Chen, Study of defect structure in ferromagnetic nanocrystalline CeO_2: effect of ionic radius, J. Phys. Chem. C 120 (2016) 14874–14882.
[28] M.M. Khan, S.A. Ansari, J.-H. Lee, M.O. Ansari, J. Lee, M.H. Cho, Electrochemically active biofilm assisted synthesis of Ag@CeO_2 nanocomposites for antimicrobial activity, photocatalysis and photoelectrodes, J. Colloid Interface Sci. 431 (2014) 255–263.
[29] N. Keshvadi, A. Haghighatzadeh, B. Mazinani, Improvement in visible-light-induced photocatalytic activity of Ag–CeO_2 Schottky-type contact heterostructures, Appl. Phys. A 256 (2020) 1–14.
[30] J. Kaur, D. Chandrakar, V. Dubey, R. Shrivastava, Y. Parganiha, N.S. Suryanarayana, Photoluminescence characteristics of dysprosium doped CeO_2 phosphor for white light emission, J. Disp. Technol. 12 (2016) 506–512.
[31] A. Ansari, Optical and structural properties of sol–gel derived nanostructured CeO_2 film, J. Semiconduct. 31 (2010), 053001.
[32] M. Alifanti, B. Baps, N. Blangenois, J. Naud, P. Grange, B. Delmon, Characterization of CeO_2-ZrO_2 mixed oxides. Comparison of the citrate and sol-gel preparation methods, Chem. Mater. 15 (2003) 395–403.
[33] R. Suresh, V. Ponnuswamy, R. Mariappan, Effect of annealing temperature on the microstructural, optical and electrical properties of CeO_2 nanoparticles by chemical precipitation method, Appl. Surf. Sci. 273 (2013) 457–464.
[34] J.G. Li, T. Ikegami, Y.Y. Wang, T. Mori, Reactive ceria nanopowders via carbonate precipitation, J. Am. Ceram. Soc. 85 (2002) 2376–2378.
[35] S.A.H. Tabrizi, M. Mazaheri, M. Aminzare, S.K. Sadrnezhaad, Reverse precipitation synthesis and characterization of CeO_2 nanopowder, J. Alloys Compd. 491 (2010) 499–502.
[36] H.-H. Ko, G. Yang, H.-Z. Cheng, M.-C. Wang, X. Zhao, Growth and optical properties of cerium dioxide nanocrystallites prepared by coprecipitation routes, Ceram. Int. 40 (2014) 4055–4064.
[37] K. Singh, R. Kumar, A. Chowdhury, Synthesis of La-doped ceria nanoparticles: impact of lanthanum depletion, J. Mater. Sci. 51 (2016) 4134–4141.
[38] T. Mokkelbost, I. Kaus, T. Grande, M.-A. Einarsrud, Combustion synthesis and characterization of nanocrystalline CeO_2-based powders, Chem. Mater. 16 (2004) 5489–5494.
[39] W. Chen, F. Li, J. Yu, Combustion synthesis and characterization of nanocrystalline CeO_2-based powders via ethylene glycol–nitrate process, Mater. Lett. 60 (2006) 57–62.
[40] L.Y. Tok, F.Y.C. Boey, Z. Dong, X.L. Sun, Hydrothermal synthesis of CeO_2 nanoparticles, J. Mater. Process. Technol. 190 (2007) 217–222.
[41] S. Dikmen, P. Shuk, M. Greenbelt, H. Gocmez, Hydrothermal synthesis and properties of $Ce_{1-x}Gd_xO_{2-i}$ solid solutions, Solid State Sci. 4 (2002) 585–590.
[42] B. Corradi, F. Bondioli, A.M. Ferrari, T. Manfredini, Synthesis and characterization of ceria powders by microwave-hydrothermal method, Mater. Res. Bull. 41 (2006) 38–44.
[43] S. Fernandez-Garcia, L. Jiang, M. Timoco, A.B. Hungria, J. Han, G. Blanco, J.J. Calvino, X. Chen, Enhanced hydroxyl radical scavenging activity by doping lanthanum in ceria nanocubes, J. Phys. Chem. C 120 (2016) 1891–1901.
[44] C. Sun, H. Li, H. Zhang, Z. Wang, L. Chen, Controlled synthesis of CeO_2 nanorods by a solvothermal method, Nanotechnology 16 (2005) 1454–1463.
[45] E. Verdon, M. Devaltte, G. Demazeau, Solvothermal synthesis of cerium oxide microcrystallites: effect of the solvent, Mater. Lett. 25 (1995) 127–131.
[46] S. Babu, R. Thanneeru, T. Inerbaev, R. Day, A.E. Masunov, A. Schulte, S. Seal, Dopant-mediated oxygen vacancy tuning in ceria nanoparticles, Nanotechnology 20 (2009), 085713.
[47] S. Patil, S. Seal, Y. Guo, A. Schulte, J. Norwood, Role of trivalent La and Nd dopants in lattice distortion and oxygen vacancy generation in cerium oxide nanoparticles, Appl. Phys. Lett. 88 (2006) 243110.
[48] G.R. Li, D.-L. Qu, L. Arurault, Y.-X. Tong, Hierarchically porous Gd^{3+}-doped CeO_2 nanostructures for the remarkable enhancement of optical and magnetic properties, J. Phys. Chem. C 113 (2009) 1235–1241.
[49] M. Krajewski, M. Michalska, B. Hamankiewicz, D. Ziolkowska, K.P. Korona, J.B. Jasinski, M. Kaminska, L. Lipinska, A. Czerwinski, $Li_4Ti_5O_{12}$ modified with Ag nanoparticles as an advanced anode material in lithium-ion batteries, J. Power Sources 245 (2014) 764–771.
[50] M. Andrzejczuk, A. Roguska, M. Michalska, A.T. Krawczyńska, L. Lipińska, A. Czerwiński, M. Cantoni, M. Lewandowska, STEM study of $Li_4Ti_5O_{12}$ anode material modified with Ag nanoparticles, J. Microsc. 264 (2016) 41–47.
[51] M. Krajewski, B. Hamankiewicz, M. Michalska, M. Andrzejczuk, L. Lipińska, A. Czerwiński, Electrochemical properties of lithium–titanium oxide, modified with Ag–Cu particles, as a negative electrode for lithium-ion batteries, RSC Adv. 7 (2017) 52151–52164.
[52] M. Michalska, A. Iwan, M. Andrzejczuk, A. Roguska, A. Sikora, B. Boharewicz, I. Tazbir, A. Hreniak, S. Popłoński, K.P. Korona, Analysis of the surface decoration of TiO_2 grains using silver nanoparticles obtained by ultrasonochemical synthesis towards organic photovoltaics, New J. Chem. 42 (2018) 7340–7354.
[53] K. Lemański, M. Michalska, M. Ptak, M. Małecka, A. Szysiak, Surface modification using silver nanoparticles of $Y_4Al_2O_9$:Nd – synthesis and their selected studies, J. Mol. Struct. 1202 (2020) 127363.
[54] https://www.imagemet.com/. (Accessed 15 October 2018).
[55] A. Sikora, Improvement of the scanning area positioning repeatability using nanomarkers developed with a nanoscratching method, Meas. Sci. Technol. 25 (2014), 055401.
[56] A. Bubnov, A. Iwan, M. Cigl, B. Boharewicz, I. Tazbir, K. Wójcik, A. Sikora, V. Hamplova, Photosensitive self-assembling materials as functional dopants for organic photovoltaic cells, RSC Adv. 6 (2016) 11577–11590.
[57] A. Iwan, A. Sikora, V. Hamplova, A. Bubnov, AFM study of advanced composite materials for organic photovoltaic cells with active layer based on P3HT:PCBM and chiral photosensitive liquid crystalline dopants, Liq. Cryst. 42 (7) (2015) 964–972.
[58] G.T. Chavan, V.M. Prakshale, S.T. Pawar, P.R. Deshmukh, A. Sikora, S.S. Kamble, N.N. Maldar, L.P. Deshmukh, Morphology improvements in CdSe thin films: a realization through mechanical agitation and incubation period, Nano-Struct. Nano-Objects 12 (2017) 113–120.
[59] M. Michalska, L. Lipińska, A. Sikora, D. Ziółkowska, K.P. Korona, M. Andrzejczuk, Structural and morphological studies of manganese-based cathode materials for lithium ion batteries, J. Alloys Compd. 632 (2015) 256–262.
[60] M. Michalska, D.A. Ziółkowska, M. Andrzejczuk, A. Krawczyńska, A. Roguska, A. Sikora, New synthesis route to decorate $Li_4Ti_5O_{12}$ grains with GO flakes, J. Alloys Compd. 719 (2017) 210–217.
[61] Y. Su, Z. Tang, W. Han, P. Zhang, Y. Song, G. Lu, Influence of the pore structure of CeO_2 supports on the surface texture and catalytic activity for CO oxidation, CrystEngComm 16 (2014) 5189–5197.
[62] Y. Yu, Y. Liu, X. Peng, X. Liu, Y. Xing, S. Xing, A multi-shelled CeO_2/Co@N-doped hollow carbon microsphere as a trifunctional electrocatalyst for a rechargeable

zinc–air battery and overall water splitting, Sustain. Energy Fuels 4 (2020) 5156–5164.
[63] Z. Fandi, N. Ameur, F.T. Brahimi, S. Bedrane, R. Bachir, Photocatalytic and corrosion inhibitor performances of CeO_2 nanoparticles decorated by noble metals: Au, Ag, Pt, J. Environ. Chem. Eng. 8 (2020) 104346.
[64] M.M. Khan, S.A. Ansari, M.O. Ansari, B.K. Min, J. Lee, M.H. Cho, Biogenic fabrication of Au@CeO_2 nanocomposite with enhanced visible light activity, J. Phys. Chem. C 118 (2014) 9477–9484.
[65] J. Makinson, J. Lee, S. Magner, R. De Angelis, W. Weins, A. Hieronymus, X-ray diffraction signatures of defects in nanocrystalline materials, Adv. X Ray Anal. 42 (2000) 407–411.
[66] M.M. Khan, S.A. Ansari, D. Pradhan, D.H. Han, J. Lee, M.H. Cho, Defect-Induced band gap narrowed CeO_2 nanostructures for visible light activities, Ind. Eng. Chem. Res. 53 (2014) 9754–9763.
[67] Q. Zhou, S. Ma, S. Zhan, Superior photocatalytic disinfection effect of Ag-3D ordered mesoporous CeO_2 under visible light, Appl. Catal., B 224 (2018) 27–37.
[68] Y. Huang, C.-F. Yan, C.-Q. Guo, S.-L. Huang, Enhanced photoreduction activity of carbon dioxide over Co_3O_4/CeO_2 catalysts under visible light irradiation, Int. J. Photoenergy (2015) 11. Article ID 230808.
[69] X. Jiao, H. Song, H. Zhao, W. Bai, L. Zhang, Y. Lv, Well-redispersed ceria nanoparticles: promising peroxidase mimetics for H_2O_2 and glucose detection, Anal. Methods 4 (2012) 3261–3267.
[70] G. Vimal, K.P. Mani, P.R. Biju, C. Joseph, N.V. Unnikrishnan, M.A. Ittyachen, Structural studies and luminescence properties of CeO_2:Eu^{3+} nanophosphors synthesized by oxalate precursor method, Appl. Nanosci. 5 (2015) 837–846.
[71] S. Pattanayak, A. Priyam, P. Paik, Facile tuning of plasmon bands in hollow silver nanoshells using mild reductant and mild stabilizer, Dalton Trans. 42 (2013) 10597–10607.
[72] R. Lopez, R. Gomez, Band-gap energy estimation from diffuse reflectance measurements on sol–gel and commercial TiO_2: a comparative study, J. Sol. Gel Sci. Technol. 61 (2012) 1–7.
[73] W.-H. Kim, W.J. Maeng, M.-K. Kim, J. Gatineau, H. Kim, Electronic structure of cerium oxide gate dielectric grown by plasma-enhanced atomic layer deposition, J. Electrochem. Soc. 158 (2011) G217–G220.
[74] A.V. Malakhovskii, A.L. Sukhachev, A.A. Leont'ev, I.A. Gudim, A.S. Krylov, A.S. Aleksandrovsky, Spectroscopic properties of $Nd_{0.5}Gd_{0.5}Fe_3(BO_3)_4$ single crystal, J. Alloys Compd. 529 (2012) 38–43.
[75] D.A. Ikonnikov, A.V. Malakhovskii, A.L. Sukhachev, A.I. Zaitsev, A.S. Aleksandrovsky, V. Jubera, Spectroscopic properties of Nd^{3+} in orthorhombic δ-BiB_3O_6 crystal, Opt. Mater. 34 (2012) 1839–1842.
[76] V.V. Atuchin, A.K. Subanakov, A.S. Aleksandrovsky, B.G. Bazarov, J.G. Bazarova, S.G. Dorzhieva, T.A. Gavrilova, A.S. Krylov, M.S. Molokeev, A.S. Oreshonkov, A.M. Pugachev, Yu.L. Tushinova, A.P. Yelisseyev, Exploration of structural, thermal, vibrational and spectroscopic properties of new noncentrosymmetric double borate $Rb_3NdB_6O_{12}$, Adv. Powder Technol. 28 (2017) 1309–1315.